Doping and Raman Characterization of Boron and Phosphorus Atoms in Germanium Nanowires

Naoki Fukata,[†,‡,*] Keisuke Sato,[†] Masanori Mitome,[†] Yoshio Bando,[†] Takashi Sekiguchi,[§] Melanie Kirkham,[⊥] Jung-il Hong,[⊥] Zhong Lin Wang,[⊥] and Robert L. Snyder[⊥]

[†]International Center for Materials Nanoarchitectonics, National Institute for Materials Science, 1-1 Namiki, Tsukuba 305-0044, Japan, [‡]PRESTO, Japan Science and Technology Agency, 4-1-8 Honcho Kawaguchi, Saitama 332-0012, Japan, [§]Advanced Electronic Materials Center, National Institute for Materials Science, 1-1 Namiki, Tsukuba 305-0044, Japan, and [⊥]School of Materials Science and Engineering, Georgia Institute of Technology, Atlanta, Georgia 30332-0245

ABSTRACT Impurity doping is the most important technique to functionalize semiconductor nanowires. The crucial point is how the states of impurity atoms can be detected. The chemical bonding states and electrical activity of boron (B) and phosphorus (P) atoms in germanium nanowires (GeNWs) are clarified by micro-Raman scattering measurements. The observation of B and P local vibarational peaks and the Fano effect clearly demonstrate that the B and P atoms are doped into the crystalline Ge region of GeNWs and electrically activated in the substitutional sites, resulting in the formation of p-type and n-type GeNWs. This method can be a useful technique for the characterization of semiconductor nanowire devices. The B-doped GeNWs showed an increasingly tapered structure with increasing B concentration. To avoid tapering and gain a uniform diameter along the growth direction of the GeNWs, a three step process was found to be useful, namely growth of GeNWs followed by the deposition of an amorphous Ge layer with high B concentration and then annealing.

KEYWORDS: germanium nanowires · boron · phosphorus · Raman scattering

A considerable amount of work has been done regarding one-dimensional semiconductor nanowires.[1−5] In particular, silicon nanowires (SiNWs) have gained attention since such SiNWs-based nanodevices are desirable for their compatibility with the present Si complementary metal-oxide semiconductors (Si CMOS) integrated circuit technology and for offering better scalability and leakage control. Ge is considered to be a more desirable material for the next-generation metal-oxide semiconductor field-effect transistors (MOSFETs), since electron and hole mobilities in Ge are higher than those in Si, indicating potential performance gains compared to Si-based devices. Indeed, GeNWs have been grown by various methods to control the growth and shape, and the electrical properties have been comprehensively investigated.[6−15] Furthermore, a core−shell structure composed of Si and Ge has been also investigated.[16,17]

Impurity doping is an important technique to form the source and drain regions in NWs-MOSFET. To form and control them, it is necessary to establish doping methods and to develop characterization methods to clarify the states of dopant atoms in NWs. Recently, the authors reported methods to detect dopant atoms in SiNWs.[18−20] In the case of B-doped SiNWs, the B local vibrational peaks were observed at about 618 cm^{-1} for ^{11}B and 640 cm^{-1} for ^{10}B by Raman scattering measurements at room temperature.[18,20] Asymmetric broadening due to the Fano effect was also observed in the Si optical phonon peak for B-doped SiNWs.[18,20] The observation of B local vibrational peaks shows that B atoms were introduced into the substitutional sites of Si atoms in the crystalline Si region of SiNWs.[18,20] The observation of Fano broadening shows that B atoms were electrically activated in the substitutional sites. These results clearly demonstrate the formation of p-type SiNWs.[18,20] The sensitivity of Raman measurements is on the order of 10^{19} cm^{-3} for both the detection of local vibrational modes and the Fano effect. On the other hand, the mass of P is very close to that of Si. This makes it difficult to detect the P local vibrational peak for P-doped SiNWs since it overlaps with the intense Si optical phonon peak. The detection of electron spins is more effective to prove the formation of n-type SiNWs, meaning that electron spin resonance (ESR) is one possible method to investigate the states of P donors in SiNWs. By performing ESR measurements at 4.2 K, an ESR signal of conduction electrons was observed for P-doped SiNWs.[19,20] This proves the formation of n-type SiNWs.[19,20] The compensation effect by codoping of B and P in SiNWs has been

*Address correspondence to fukata.naoki@nims.go.jp.

Received for review February 15, 2010 and accepted June 15, 2010.

Published online June 21, 2010.
10.1021/nn100734e

also shown by the authors.[21] No similar results have been reported for GeNWs. The mass of B and P are different from that of Ge. This makes it possible to detect the local vibrational peaks of B and P by the same Raman scattering measurements, contrary to that in the case of SiNWs.

In this paper, we report the impurity doping of B and P in GeNWs and the detection of Raman peaks related to B and P. These results clarify the states of dopant atoms in GeNWs and clearly demonstrate the formation of p-type and n-type GeNWs. We also show a specific method of B doping and structural control for B-doped GeNWs.

RESULTS AND DISCUSSION

The scanning electron microscopy (SEM) and transmission electron microscopy (TEM) images of typical undoped, B-doped, and P-doped GeNWs are shown in Figure 1. The SEM image of undoped GeNWs in Figure 1a demonstrates that the diameter is uniform along the length of the GeNWs. The main growth direction is [110] for GeNWs with a diameter smaller than about 20 nm, and [111] for GeNWs with a diameter larger than 20 nm. This is the same tendency as has been observed in SiNWs.[22,23] The TEM images of undoped GeNWs in Figure 1i,j show that the core is crystalline Ge and the surrounding layer is amorphous GeO_2 approximately 2 nm in thickness. The diameter of P-doped GeNWs does not significantly depend on the PH_3 gas ratio, resulting in a uniform diameter as shown in Figure 1g,h. On the other hand, the shape of the B-doped GeNWs strongly depends on the ratio of B_2H_6 gas to GeH_4 gas during the growth. The shape changes with increasing B_2H_6 gas (decreasing partial pressure of GeH_4 gas) and finally shows cone-like structures for the case of B_2H_6 gas of 2.2 sccm as shown in Figure 1f. Hereafter, we call the cone-like structures Ge microcones (GeMCs) to distinguish them from GeNWs with uniform diameter along the length of the NWs. A similar result has been reported by Tutuc *et al.*[7] The presence of B_2H_6 gas causes the radial growth, resulting in cone-like tapering structures. The radial growth layer is crystalline Ge as shown in Figure 1l. Previous studies of SiNWs showed that a SiNW with a ⟨110⟩ axis has a hexagonal cross section with well-developed facets, corresponding to the low-free-energy {111} and {100} planes.[23,24] Our results indicate that GeMC with a ⟨110⟩ axis also has facets composed of {111} and {100} planes as shown in the inset of Figure 1f. The surfaces of the highly B-doped GeMC are not smooth but rather rough. One of the reasons is the high growth rate assisted by B_2H_6 gas at the low growth temperature of 300 °C. Generally, epitaxial growth of Ge on Si or Ge substrates is performed at around 600 °C. Low growth rate and high growth temperature are important for the migration of Ge atoms and 2-dimentional layer-by-layer epitaxial growth. A high growth rate at a low temperature significantly disturbs the migration of Ge atoms on the surface of Ge nanowires, resulting in three-dimensional island-based growth. The Stranski−Krastanov growth mode is also known for three-dimensional island-based growth. This growth occurs in the case of heteroepitaxial growth with stress due to lattice mismatch. The case of B-doped GeMC is due to homoepitaxy. On the basis of these points, the rough surface is probably caused by the high growth rate assisted by B_2H_6 gas at a low growth temperature if there is no stress during the side growth. The TEM image of the top of GeMC in Figure 1k shows that dark regions are observed in addition to the Au catalytic nanoparticles. These dark regions were found to be due to Au from energy dispersive X-ray (EDX) analysis (see Supporting Information). This is due to the Au surface diffusion during the growth, and similar

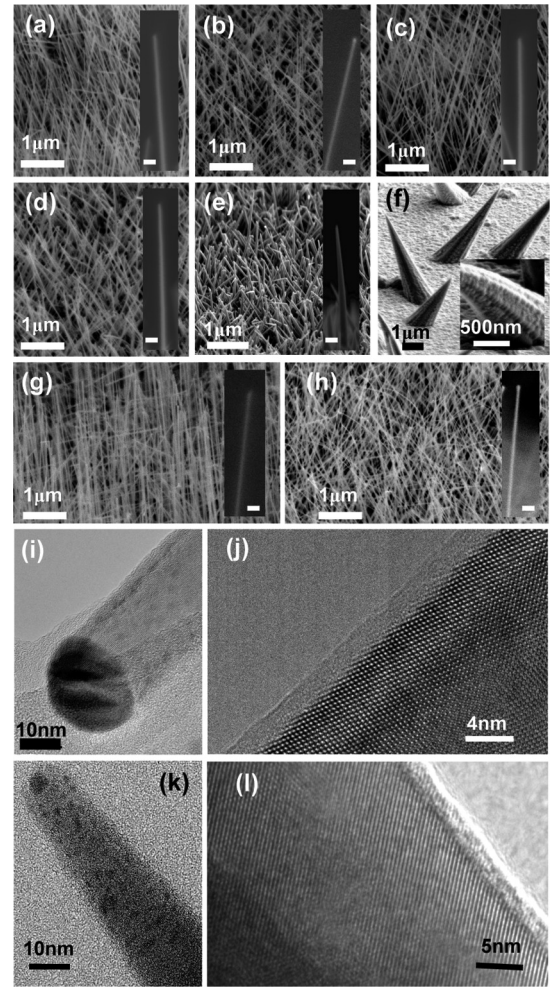

Figure 1. SEM images of GeNWs synthesized by CVD with gas mixtures with ratios of GeH_4 to B_2H_6 of (a) 10:0, (b) 10:0.2, (c) 10:0.4, (d) 10:0.7, (e) 10:1.0, and (f) 10:2.2. The insets show the magnification of single NWs. The scale bar is 20 nm. SEM images of GeNWs synthesized by CVD with gas mixtures with ratios of GeH_4 to PH_3 of (g) 10:1.0 and (h) 10:7.0. The insets show the magnification of single NWs, and the scale bars are 30 nm. TEM images of GeNWs synthesized by CVD with gas mixtures with a ratio of GeH_4 to B_2H_6 of (i) 10:0 and (k) 10:2.2. Panels j and l are the high resolution TEM images of panels i and k, respectively.

results have been observed in other NWs.[25−27] Residual Au atoms on the surface and an amorphous GeO_2 shell do not affect the Raman results. They also do not affect the peak position of the Ge optical phonon peak, B local vibrational peaks, and P local vibrational peaks. However, they do affect the Fano line shape because Au atoms induce deep levels in the band gap of Ge nanowires and compensate the dopant carriers. This causes a decrease in the carrier concentration, resulting in a decrease in the Fano broadening. In this study, Au distribution was only seen at the top of NWs as the black points, showing that the effect of the compensation is small.

To prove B acceptor doping in GeNWs, we performed micro-Raman scattering measurements at room temperature (RT). The Raman measurements were performed not for a single nanowire but rather several tens of nanowires at the same time. Hereafter, we mainly explain the results of Raman measurements for B-doped GeNWs with uniform diameter (GeH_4:B_2H_6 = 10:0.1−0.7) and slightly tapered B-doped GeNWs (GeH_4:B_2H_6 = 10:1.0) because the GeMCs are not appropriate for device applications. The results were shown in Figure 2a,b. The intense peak at about 300.2 cm^{-1} for bulk-Ge is due to the Ge optical phonon peak. Two peaks at about 544 and 565 cm^{-1} were observed for B-doped GeNWs. The intensity increased with increasing B_2H_6 gas ratio. The peak position of the latter peak is close to that of the second-order Ge optical phonon peak. However, there is no correlation between the intensity of the first-order Ge optical phonon peak and that of the second-order Ge optical phonon peak. This indicates the overlapping of other peaks. In our previous study, the B local vibrational peaks were observed at about 618 cm^{-1} for ^{11}B and 640 cm^{-1} for ^{10}B for B-doped SiNWs.[18] The intensity ratio of the two peaks is estimated as being roughly 4:1, which is in good agreement with the natural abundance of the two isotopes of ^{11}B (80.2%) and ^{10}B (19.8%). These results proved the B acceptor doping in SiNWs, that is, B atoms were doped in the substitutional sites of Si atoms in crystalline Si region of SiNWs. If Si atoms were replaced by Ge atoms, the B local vibrational peaks shifted to around 540−580 cm^{-1}. The peaks at about 544 and 565 cm^{-1} are in this frequency range. On the basis of the dependence on the B_2H_6 gas ratio and the peak position, the peak at 544 cm^{-1} can be assigned to the ^{11}B local vibrational peak in GeNWs, while the peak at 565 cm^{-1} is probably due to the overlapping peak of the ^{10}B local vibrational peak and the second-order Ge optical phonon peak. The intensity ratio of the peak at 544 cm^{-1} to that at 565 cm^{-1} is roughly estimated to be about 4:1 after removing the effect of the second-order Ge optical phonon peak. The value is in agreement with the natural abundance of B isotopes. These results clearly demonstrate B acceptor doping in GeNWs, that is, B atoms were doped into the substitutional sites

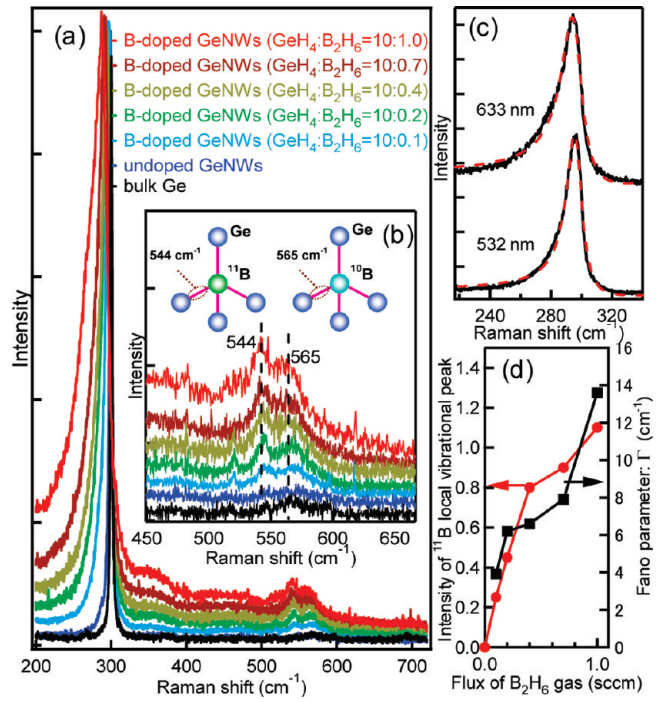

Figure 2. (a) Raman spectra observed for B-doped GeNWs (B_2H_6 flux of 1.0, 0.7, 0.4, 0.2, and 0.1, starting from the top), undoped GeNWs (the second from the bottom), and bulk Ge (bottom). (b) Magnification of the Raman spectra ranging from 200 to 700 cm^{-1}. (c) Dependence of the line shapes of the Ge optical phonon peak on the excitation wavelength (GeH_4:B_2H_6 = 10:0.2). The dotted red lines are fitting curves by the Fano equation. (d) Dependence of the intensity of ^{11}B local vibrational peak and the Fano fitting parameter (Γ) on the flux of B_2H_6 gas. B-doped GeNWs and undoped GeNWs were grown at 300 °C.

of Ge atoms in the crystalline Ge region of GeNWs. A broad band was observed between 300 and 400 cm^{-1} for highly B-doped GeNWs. However, the origin of the band is not clear.

As seen in Figure 2, the optical phonon peak observed for undoped GeNWs showed a downshift of 0.6 cm^{-1} and a broadening toward lower wavenumber compared with the case of bulk Ge. This is due to the phonon confinement effect caused by the small diameter of GeNWs.[28,29] The diameter of crystalline Ge core for undoped GeNWs is estimated to be about 15 nm by fitting the Ge optical phonon peak using the phonon confinement model.[28−30] The value is in good agreement with the experimental result shown in Figure 1i. The down shift and asymmetric broadening toward lower wavenumber became more pronounced with increasing B_2H_6 gas ratio. This is attributable to the Fano interference, which is due to coupling between discrete optical phonons and the continuum of interband hole excitations in degenerately doped p-type Ge.[31,32] According to a previous study about highly B-doped bulk Ge, Raman scattering is enhanced on the low-wavenumber side of the Ge optical phonon peak (constructive interference) and suppressed on the high-wavenumber side of the peak (destructive interference).[33] The latter is also called antiresonance. The

TABLE 1. Fitting Parameters for the Fano Line Shapes of the Ge Optical Phonon Peak Observed for B-Doped GeNWs with 532-nm and 633-nm Excitation Lights. SSR Is the Sum of Squares of the Residuals

B_2H_6 (sccm)	*q*: 532 nm	Γ (cm^{-1}): 532 nm	SSR	*q*: 633 nm	Γ (cm^{-1}): 633 nm	SSR
0.1	−7.2	3.9	1.1×10^{-1}	−5.8	4.1	5.3×10^{-1}
0.2	−6.4	6.2	2.3×10^{-1}	−4.6	8.1	5.9×10^{-1}
0.4	−4.8	6.6	1.5×10^{-1}	−4.4	12.8	2.1×10^{-1}
0.7	−3.9	7.9	1.4×10^{-1}	−3.6	15.6	3.5×10^{-1}
1.0	−3.6	13.6	3.0×10^{-1}	−3.4	17.3	3.7×10^{-1}

TABLE 2. Fitting Parameters for the Fano Line Shapes of the Ge Optical Phonon Peak Observed for P-Doped GeNWs with 532-nm and 633-nm Excitation Lights. SSR Is the Sum of Squares of the Residuals

PH_3 (sccm)	*q*: 532 nm	Γ (cm^{-1}): 532 nm	SSR	*q*: 633 nm	Γ (cm^{-1}): 633 nm	SSR
0.1	−22.4	2.1	1.6×10^{-2}	−16.1	2.2	1.7×10^{-2}
0.4	−18.7	2.3	1.7×10^{-2}	−12.6	2.4	2.3×10^{-2}
0.7	−17.0	2.4	1.9×10^{-2}	−11.0	2.5	2.3×10^{-2}
1.4	−13.9	2.5	1.7×10^{-2}	−7.7	2.8	2.2×10^{-2}
4.0	−13.7	2.6	2.2×10^{-2}	−6.7	3.0	2.5×10^{-2}
7.0	−13.5	2.6	1.7×10^{-2}	−6.3	3.1	1.9×10^{-2}

results from B-doped GeNWs in Figure 2a show the same tendency. To confirm the observation of the Fano interference, we investigated the dependence of Raman line shapes on the excitation wavelength. Generally, the Fano interference depends on the excitation wavelength. The Ge optical phonon peak showed a large broadening to a lower wavenumber with increasing excitation wavelength as shown in Figure 2c. This result shows that the asymmetric broadening is surely due to the Fano interference and that B atoms are electrically activated in the crystalline Ge region of the GeNWs. The dependence of the asymmetric broadening and the peak intensity of ^{11}B also show a good correlation as shown in Figure 2d. On the basis of the observation of the B local vibrational peak and the Fano interference in the Ge optical phonon peak, we have clearly demonstrated the formation of B-doped p-type GeNWs. We also analyzed the Ge optical phonon peak by the Fano equation.[31,32] The asymmetric line shape of the phonon is given by

$$I(\omega) = I_0 \frac{(q + \varepsilon)^2}{(1 + \varepsilon^2)} \quad (1)$$

where ω is the wavenumber, I_0 is the prefactor, *q* is the asymmetry parameter, and ε is given by $\varepsilon = (\omega - \omega_p)/\Gamma$, where ω_p is the phonon wavenumber and Γ is the line width parameter. The fitting results of B-doped GeNWs excited with a 532-nm light are summarized in Table 1. The results of excitation with a 633-nm light are also shown in Table 2. As already described in the explanation of Figure 2c, the increase in *q* and Γ for the longer excitation wavelengths shows that the asymmetric broadening is due to the Fano interference. The values of *q* and Γ depend on the electrical activity of dopant atoms. By comparing with the parameters for bulk Ge, the electrical active dopant concentrations can be roughly deduced. The values of *q* and Γ were estimated to be about −3.9 and 7.9, respectively, for B-doped GeNWs (GeH_4:B_2H_6 = 10:0.7). These values are larger than in the case of bulk Ge doped with a B concentration of 5.5×10^{19} cm^{-3},[32] suggesting that the electrical active B concentration is probably on the order of 10^{20} cm^{-3}. In this analysis, however, we ignored the effect of phonon confinement, meaning that the values slightly overestimate the Fano interference. The Raman spectrum of B-doped GeNWs (GeH_4:B_2H_6 = 10:0.4) is much broader than that of B-implanted Ge (5×10^{16} B^+ cm^{-2}), suggesting the heavy B doping in GeNWs as shown in Figure 3a. Indeed, the result of secondary ion mass spectrometry (SIMS) measurements in Figure 3b shows that the B concentration is about $2-3 \times 10^{20}$ cm^{-3} for the case of B-doped GeNWs (GeH_4:B_2H_6 = 10:0.4). The depth profile of B shows the abrupt decrease from 0.3 μm. Si atoms were not detected before the decrease, showing that the depth profile before the decrease corresponds to those in GeNWs. We used the depth profile before the decrease to discuss the con-

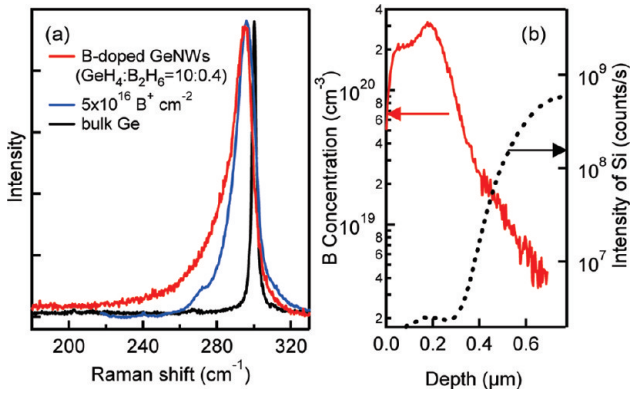

Figure 3. (a) Raman spectra observed for B-doped GeNWs (GeH_4:B_2H_6 = 10:0.4), bulk Ge implanted with a dose of 5×10^{16} B^+ cm^{-2}, and bulk Ge without B implantation from the top. (b) B concentration profiles of B-doped GeNWs (GeH_4:B_2H_6 = 10:0.4). The Si concentration profile is also shown as dotted line.

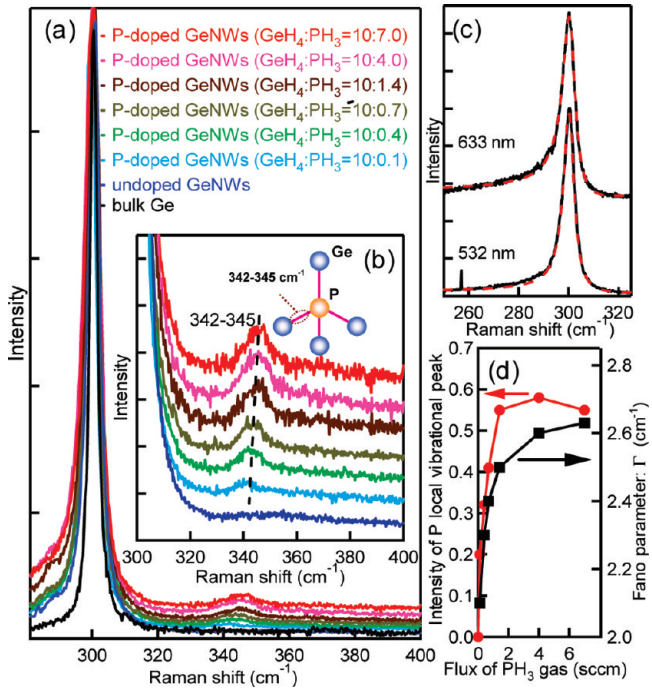

Figure 4. (a) Raman spectra observed for P-doped GeNWs (PH_3 flux of 7.0, 4.0, 1.4, 0.7, 0.4, and 0.1, starting from the top), undoped GeNWs (the second from the bottom), and bulk Ge (bottom). (b) Magnification of the Raman spectra ranging from 300 to 400 cm^{-1}. (c) Dependence of the line shapes of the Ge optical phonon peak on the excitation wavelength (GeH_4:PH_3 = 10:7.0). The dotted red lines are fitting curves by the Fano equation. (d) Dependence of the intensity of P local vibrational peak and the Fano fitting parameter (Γ) on the flux of PH_3 gas. P-doped GeNWs and undoped GeNWs were grown at 350 and 300 °C, respectively.

centration of B in GeNWs. As already described in experimental section, the concentration and depth have some uncertainty since the samples of NWs are not a continuous solid. On the basis of these results, the electrical active B concentration in GeNWs is probably on the order of 10^{20} cm^{-3}. In the Raman spectrum of B-implanted Ge (5×10^{16} B^+ cm^{-2}), a shoulder peak was observed at around 270 cm^{-1}. The peak may be due to a residual amorphous region induced by implantation.

The result of micro-Raman scattering measurements for P-doped GeNWs is shown in Figure 4. Unlike the B-doped GeNWs, a peak was observed at about 342−345 cm^{-1}. The peak intensity increased with increasing PH_3 gas ratio as shown in Figure 4 panels a and b. The frequency of the P local vibrational peak can be roughly estimated in a similar way to the estimation of the B local vibrational peaks for B-doped GeNWs. By replacing a B atom with a P atom, the peak at 544 cm^{-1} shifts to around 360 cm^{-1}. The estimated value is in good agreement with the experimental value of 342−345 cm^{-1}. Considering the dependence of the peak intensity on the PH_3 gas ratio and the peak frequency, the peak at 342−345 cm^{-1} can be assigned to the local vibrational peak of P in GeNWs. Here, the peak frequencies seemed to slightly shift with the PH_3 gas ratio. This is probably due to the effect of stress introduced by the incorporation of a high concentration of P.

The Ge optical phonon peak also showed a downshift and an asymmetric broadening for P-doped GeNWs, as shown in Figure 4. The downshift and asymmetric broadening toward lower wavenumber became more pronounced with increasing PH_3 gas ratio similar to the case observed for B-doped GeNWs. There are no reports about Fano interference for P-doped bulk Ge. To prove the Fano interference, we investigated the dependence of Raman line shapes on the excitation wavelength for P-doped GeNWs. The Ge optical phonon peak showed a larger broadening to lower wavenumber for the longer excitation wavelength as shown in Figure 4c. This can be well explained by the Fano interference. To further check the Fano interference for P-doped bulk Ge, P ion implantation was performed for bulk Ge as shown in Figure 5a. The result showed a similar line shape to that for P-doped GeNWs. The concentration of P in GeNWs will be explained later. The dependence of the asymmetric broadening and the peak intensity of the P local vibrational peak also show a good correlation as shown in Figure 4d. On the basis of the observation of the P local vibrational peak and the Fano interference in the Ge optical phonon peak, we have also clearly demonstrated the formation of P-doped n-type GeNWs. In the Raman spectrum of P-doped GeNWs (GeH_4:PH_3 = 10:1.4) shown in Figure 4a, a shoulder peak was observed at around 290 cm^{-1}. The origin of the peak is not clear at the present time. In the case of SiNWs, a peak at 503 cm^{-1} is sometimes observed at the

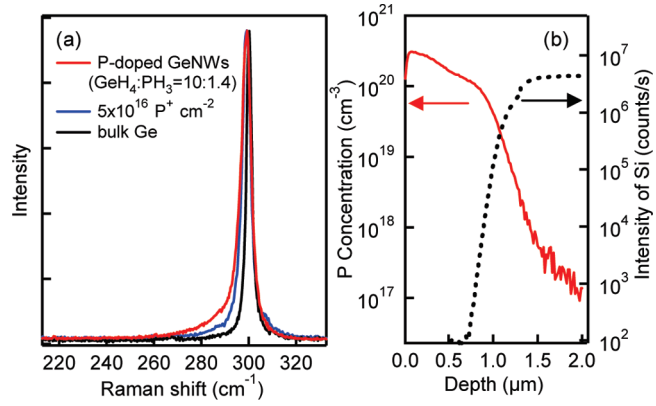

Figure 5. (a) Raman spectra observed for P-doped GeNWs (GeH_4:PH_3 = 10:1.4), bulk Ge implanted with a dose of 5×10^{16} P^+ cm^{-2}, and bulk Ge without P implantation from the top. (b) P concentration profile of P-doped GeNWs (GeH_4: PH_3 = 10:7.0). The Si concentration profile is also shown as a dotted line.

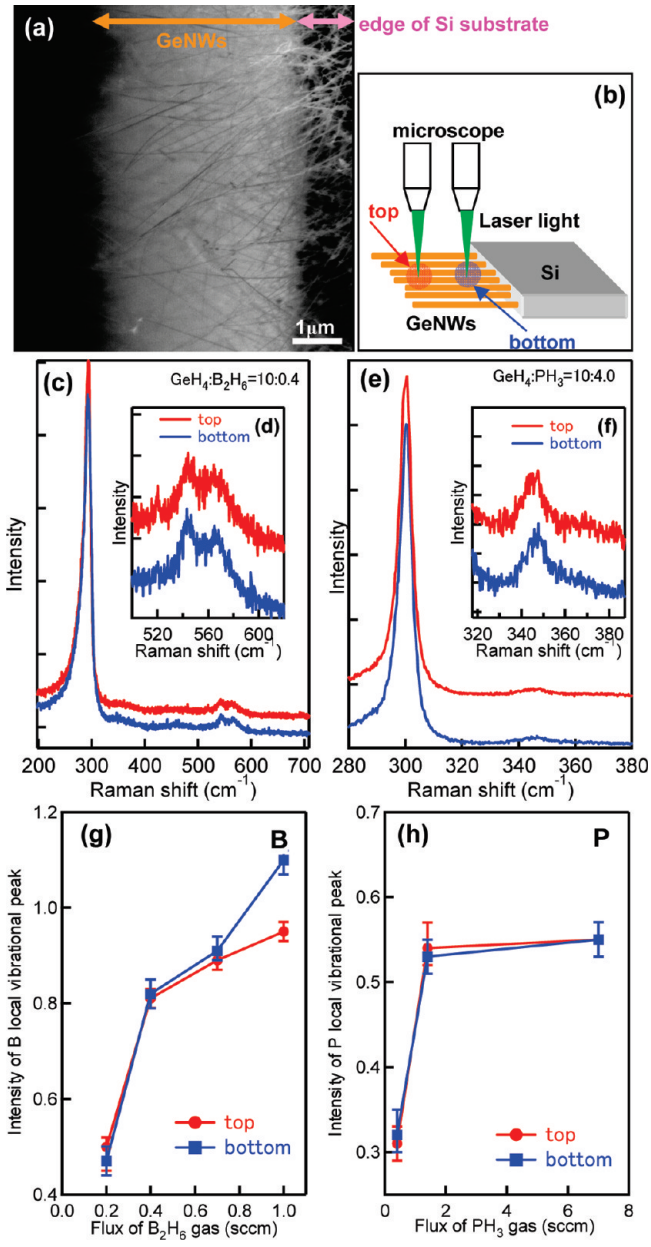

Figure 6. (a) SEM image of B-doped GeNWs (GeH_4:B_2H_6 = 10:0.4) grown at the edge of Si substrate. (b) Illustration of Raman measurements of GeNWs grown at the edge of Si substrate. (c) Raman spectra observed for the top (red) and the bottom (blue) regions of B-doped GeNWs (GeH_4:B_2H_6 = 10:0.4). Inset d is a magnification of panel c. (e) Raman spectra observed for the top (red) and the bottom (blue) regions of P-doped GeNWs (GeH_4:PH_3 = 10:4.0). Inset f is a magnification of panel e. (g) Dependence of the intensity of B local vibrational peak on the flux of B_2H_6 gas. (h) Dependence of the intensity of P local vibrational peak on the flux of PH_3 gas.

shoulder of the Si optical phonon peak at 520 cm^{-1}. The origin of the peak at 503 cm^{-1} has been already assigned to an optical phonon peak related to the wurtzite structure of Si.[33] The wurtzite structure may also be the origin of the shoulder peak observed for GeNWs.

We also analyzed the Ge optical phonon peak observed for P-doped GeNWs by the Fano equation.[31,32] The results of P-doped GeNWs are summarized in Table 2. The values of q and Γ increased with increasing excitation wavelength, showing that the asymmetric broadening is due to the Fano interference. The Ge optical phonon peak of P-doped GeNWs (GeH_4:PH_3 = 10:1.4) is almost the same as that of the P-implanted Ge (5×10^{16} P^+ cm^{-2}) as shown in Figure 5a. The result of SIMS measurements in Figure 5b shows that the P concentration is about 2×10^{20} cm^{-3} for the case of P-doped GeNWs (GeH_4:PH_3 = 10:7.0). Considering the above-mentioned results, the P concentration in GeNWs (GeH_4:PH_3 = 10:1.4−7.0) is probably in the order of 10^{20} cm^{-3}. Fano broadening observed for P-doped GeNWs is weaker compared with that observed in the case of B-doped GeNWs. This can be explained by the efficiency of the interference. It is known that the Fano interference for n-type Si is weaker than that for p-type Si[34,35] since Fano interference in p-type Si is effectively caused by interband hole excitations between occupied light holes and unoccupied heavy holes. The same tendency applies to the case of Ge and GeNWs, resulting in smaller Fano broadening in n-type Ge than in p-type Ge.

To investigate the effect of shell doping, we performed position dependent Raman measurements for the top and bottom regions of B- or P-doped GeNWs grown at the edge of the Si substrate as shown in Figure 6b. The SEM image of B-doped GeNWs (GeH_4:B_2H_6 = 10:0.4) is shown in Figure 6a. First, we performed Raman measurements at the bottom regions of B-doped and P-doped GeNWs and then precisely moved to top regions by using a micrometer of the specimen stage. To get Raman peaks, we increased accumulation time during Raman measurements. The results of Raman measurements are summarized in Figure 6c−h. The numbers of GeNWs are different by location. To remove the effect, the intensity of B and P local vibrational peaks were normalized by the Ge optical phonon peak. We performed 20 Raman measurements at the top and bottom regions, respectively. As shown in Figure 6c,d,g, the intensity of the B local vibrational peak does not show big differences up to the B_2H_6 gas flux of 0.4 sccm, while the intensity of the bottom region is slightly larger than that of the top region at 0.7 sccm; finally the former is clearly larger than the latter at 1.0 sccm. This result shows that the effect of shell doping has to be considered from the B_2H_6 gas flux more than 0.7 sccm; that is, the Fano parameters estimated for the B_2H_6 gas flux more than 0.7 sccm shown in Table 1 probably include the effect of the shell doping. Indeed, the SEM image of Figure 1e (GeH_4:B_2H_6 = 10:1.0) clearly shows tapered structure, and the tapered structure is a proof of the radial growth and shell doping. On the other hand, the intensity of the P local vibrational peak does not show big differences. On the basis of these results, we could show that the effect of shell doping can be clearly detected for tapered

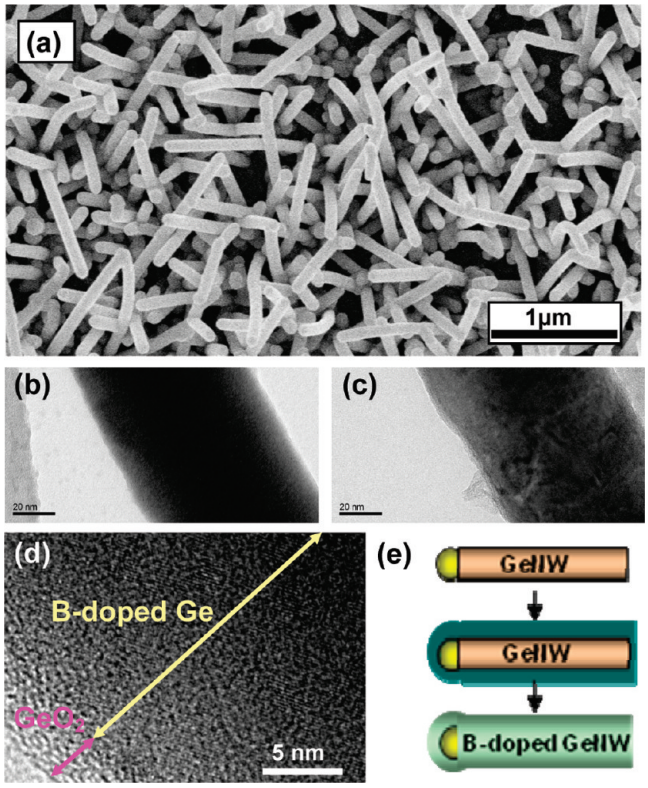

Figure 7. (a) SEM images of B-doped rod-type GeNWs before annealing. TEM images of B-doped rod-type GeNWs (b) before and (c) after annealing at 800 °C for 30 min. (d) High-resolution of TEM image of panel c. (e) Illustration of the formation process of B-doped rod-type GeNWs with uniform diameters. The growth of GeNWs and the lateral deposition of amorphous Ge layers with high B concentration by were performed at 300 °C.

GeNWs by position-dependent Raman measurements. Core doping is considered as another doping mechanism. The results of Figure 6 showed that the Raman intensities at the top and bottom regions are coincident with each other within the margin of error. However, this is not conclusive enough to prove only the core doping for untapered nanowires. Shell doping is one of the general doping processes in nanowires and has to be considered even for untapered nanowires. In addition to this, the effective penetration depth of 532 nm light is about 20 nm. The diameter of untapered GeNWs is around 20 nm. The distribution of diameters in the Raman measurement range affects the results of position-dependent Raman measurements. On the basis of these points, both shell and core doping are considered for B and P doping in GeNWs at the present time.

Finally, we investigated B-doping after the growth of GeNWs. The introduction of B_2H_6 gas strongly affects the growth of GeNWs, resulting in the cone-like structure shown in Figure 1e,f. To avoid the structure change and to obtain a uniform diameter along the length of the GeNWs even with high B doping, B doping was performed by three steps as illustrated in Figure 7e. The first step is the growth of GeNWs by chemical vapor deposition (CVD) using GeH_4 gas. The second step is lateral deposition of an amorphous Ge layer with high B concentration by immediately introducing B_2H_6 gas after stopping the GeH_4 gas. The existence of residual GeH_4 gas effectively works to form a thick amorphous layer with high B concentration. The third step is annealing at 800 °C to crystallize the surface deposition layer and to electrically activate the B and/or to dope B into the initial core GeNWs. A similar experiment has been reported by Greytak *et al.*[11] In their study, GeNWs were surface-doped *in situ* using B_2H_6 gas, and then radial growth of an epitaxial Ge shell was used to cap the dopant layer. The SEM images after surface deposition is shown in Figure 7a. Contrary to the result of Figure 1e,f, the SEM image of Figure 7a clearly shows the formation of rod-type structures with uniform diameter. The reason why thick rod-type structures were used instead of thin nanowires is as follows. The doping of impurity atoms into GeNWs is much more difficult than that into bulk Ge because of the self-purification effect.[36,37] In addition to this, a thin amorphous Ge layer with high B concentration was easily evaporated from the surface during thermal annealing. To increase the doping probability, we deposited thick layers on the surfaces of GeNWs. The TEM images before and after annealing are shown in Figure 7b,c. The high-resolution TEM image in Figure 7d collected after annealing shows the Ge lattice fringes in the rod-type GeNW, while no Ge lattice fringes were observed before annealing. This is due to the effect of blocking and charging by the thick amorphous layers.

To investigate the crystal structure of the above-mentioned B-doped rod-type GeNWs through the surface deposition layer, X-ray diffraction (XRD) measurements were performed at room temperature before and after annealing. Figure 8 panels a and b show the result before annealing. The pattern shows the peaks representing the (111), (220), (311), and (511) crystallographic planes of the cubic diamond structure, indicating that the cores of the GeNWs are crystalline. Figure 8c shows a magnification of the Ge(111) peak before and after annealing. The peak position of the Ge(111) before annealing is the same as that observed for undoped GeNWs, showing no stress in the Ge core region by the deposition of the amorphous Ge layer with high B concentration. The Ge(111) peak shows a shift to a higher angle after annealing. The average lattice constant of B-doped

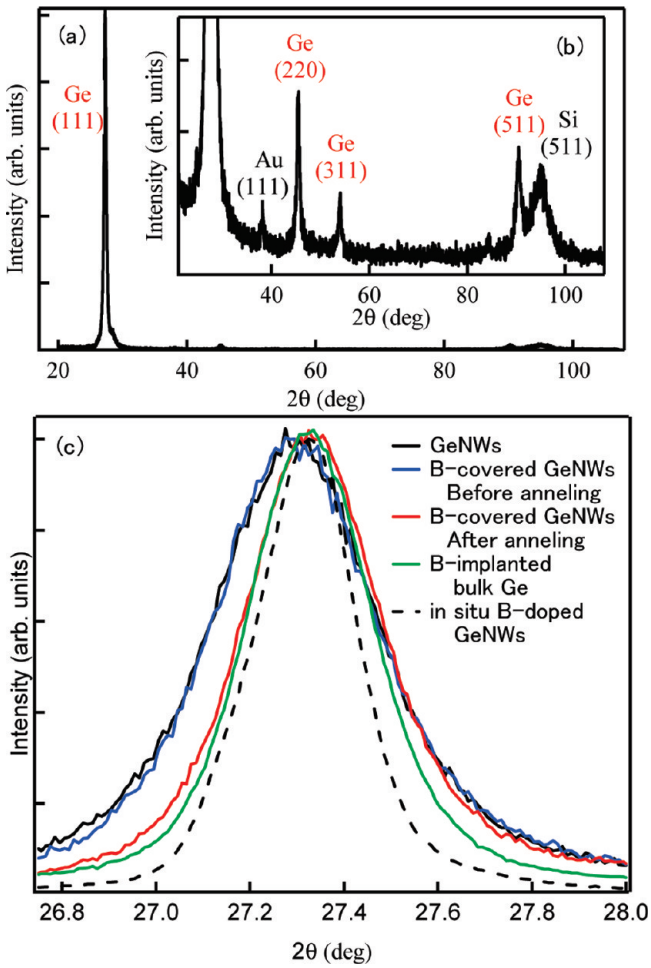

Figure 8. (a) XRD pattern obtained for B-doped rod-type GeNWs. (b) Magnification of the Ge-related peaks. (c) XRD peak of Ge(111) before and after annealing at 750 °C. The XRD patterns for undoped GeNWs, *in situ* B-doped GeNWs (GeH_4:B_2H_6 = 10:2.2), and B-implanted bulk Ge are also shown. B implantation was performed at 30 keV with 5 × 10^{16} B^+/cm^2 and the implanted specimen was annealed at 800 °C for 30 min.

rod-type GeNWs is determined to be 5.647 ± 0.002 Å, while that of undoped GeNWs is 5.660 ± 0.002 Å, showing that lattice contraction in the GeNWs results from the substitution of B atoms into the Ge lattice. The same tendency is observed for B-implanted bulk Ge and *in situ* B-doped GeNWs (GeH_4:B_2H_6 = 10:2.2) as shown in Figure 8c.

To further confirm the B doping after annealing, we performed Raman measurements. The results are shown in Figure 9a,b. A broad peak was observed at about 277 cm^{-1} before annealing. The peak position is much lower and the peak width is much broader than that of GeNWs shown in Figure 2. This is due to the deposition of thick amorphous layers surrounding with GeNWs. The thick amorphous Ge layer with high B concentration probably disturbed the Raman measurements of the crystalline Ge core of GeNWs. The thick amorphous layer also disturbed the observation of Ge lattice fringes by TEM. The peak at about 277 cm^{-1} became larger and shifted to 294 cm^{-1} with increasing annealing time, indicating that B atoms in the surface deposition layer were electrically activated and/or introduced into Ge core of GeNWs. In addition to this, the small B local vibrational peak was observed after annealing, showing the formation of p-type GeNWs. The intensities of B local vibrational peaks are lower than that of the second-order Ge optical phonon peak. Therefore, the intensity ratio of the two peaks at 544 and 565 cm^{-1} may seem different from that in Figure 2, but in substance they are the same if the effect of the second-order Ge optical phonon peak is removed. These results indicate that three step doping is a useful technique for B acceptor doping in GeNWs with a uniform diameter along the growth direction. Comparing the intensities of the B local vibrational peaks, the B concentration in B-doped rod-type GeNWs grown in the three step process is roughly estimated to be less than 5 × 10^{19} cm^{-3}, lower than the B concentration when grown in a single step process ((GeH_4:B_2H_6 = 10:0.4)). This result suggests that B doping after VLS growth is more difficult than during VLS growth. In the future, it will be necessary to investigate the distributions of dopant atoms with radial and axial directions of GeNWs to clarify the location of dopant atoms.[38]

CONCLUSIONS

B- acceptor and P-donor doping in GeNWs during CVD were confirmed by the observation of local vibrational peaks of ^{11}B, ^{10}B, and P at about 544, 565, and 342−345 cm^{-1}, respectively, using Raman scattering measurements. The electrical activities were verified by the Fano broadening in the Ge optical phonon peak. The effect of shell doping was clearly detected for tapered GeNWs by position dependent Raman measurements. Core doping is also considered as another im-

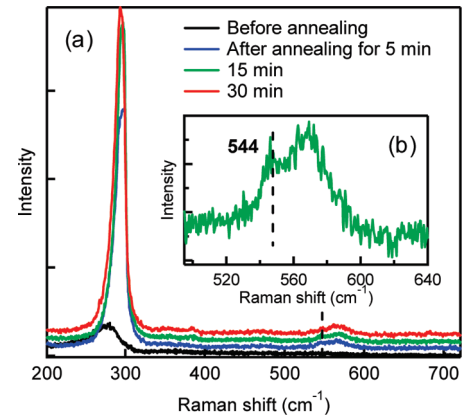

Figure 9. (a) Annealing behaviors of Raman spectra observed for GeNWs doped with B by a three-step process. The annealing times are 0, 5, 15, and 30 min, respectively, starting from the top. (b) Magnification of Raman spectrum observed after annealing for 15 min.

portant doping mechanism, and both mechanisms for B and P doping in GeNWs are considered at the present time to be possible. The concentration of B acceptors and P donors can be roughly controlled by the B_2H_6 and PH_3 gas flux, respectively. The three-step process is effective for B doping to avoid the formation of a tapered structure and to gain a uniform diameter along the length of the GeNWs.

EXPERIMENTAL SECTION

Growth of GeNWs. We grew GeNWs with high density and long length on Si(111) substrates to suppress the Si substrate effect on Raman and SIMS measurements. GeNWs were grown on a Si(111) substrate by chemical vapor deposition (CVD) using 10 sccm of GeH_4 (100%). The total pressure was set at 8 Torr by mixing with N_2 gas (30 sccm). Doping with B and P was performed during the growth. Diborane (1% B_2H_6 in H_2) was used for the p-type dopant and phosphine (1% PH_3 in H_2) for the n-type dopant. Gold nanocolloid particles 3 nm in diameter were used as seeds for vapor−liquid−solid (VLS) growth of GeNWs. The Si(111) substrates were etched with a 1% HF solution before the deposition of gold nanocolloid particles. The substrates with the gold nanocolloids were heated to 300 °C for nondoping and B doping cases, and 350 °C for the P doping case. After the growth temperature was reached, the gases were introduced into the chamber. In addition to *in situ* doping, B doping was performed by a three step process: (1) growth of GeNWs by CVD using GeH_4 gas, (2) lateral deposition of an amorphous Ge layer with high B concentration by immediately introducing B_2H_6 gas after stopping the GeH_4 gas, and (3) annealing at 800 °C. We also used Ge bulk wafers implanted at 30 keV with 5×10^{16} B^+/cm^2 and 80 keV with 1×10^{17} P^+/cm^2, respectively. These implanted specimens were annealed at 800 °C for 30 min to electrically activate the dopant atoms.

Characterization Methods. Micro-Raman scattering measurements were performed to investigate the states of dopant atoms in GeNWs at room temperature with a 100× objective and a 532-nm excitation light. We also performed Raman measurements with a 633-nm excitation light to prove Fano interference. The penetration depth of 532 and 633-nm excitation light is about 20 and 30 nm, respectively. The excitation power was set to be about 0.02 mW to avoid local heating effects due to the excitation laser.[39,40] The spectral resolution of all data is about 0.3 cm^{-1}. We grew GeNWs on Si substrates, not Ge substrates. By using Si substrates, we can completely remove the effect of the substrate. In the case of Raman measurements, the peak positions of B and P local vibrational peaks for Ge are different from those for Si. The peak position of the Ge optical phonon is also different from that of the Si optical phonon peak (520 cm^{-1}), showing that the Fano broadening observed in this study is due to electrically active B and P in GeNWs. SEM (scanning transmission electron microscopy) (Hitachi, S-4300, 3 kV) and TEM (transmission electron microscopy) (JEOL, JEM4000EX: 400 kV) were used to observe the GeNWs and to investigate their detailed structures. Energy dispersive X-ray analysis (EDX) measurements were also performed in the TEM to investigate the chemical content of the GeNWs. Concentrations of the B and P atoms in GeNWs were measured using SIMS using primary Cs^+ and O_2^+ beams with an energy of 15.0 kV normal to the samples. The concentrations in the vertical axis were determined by comparison with a B^+ or P^+ ion-implanted Ge bulk wafer. The estimated concentrations and depth have some uncertainty since the samples of NWs are not a continuous solid. The Si depth profiles were also measured at the same time in order to check the position of the Si substrate. XRD measurements were performed to investigate the crystal structure of the GeNWs. XRD data were collected with Cu Kα radiation and parallel beam optics on a Panalytical X'Pert Pro MRD.

Acknowledgment. This work was supported by the Japan Science and Technology Agency (JST) and World Premier International Research Center Initiative (WPI Initiative), MEXT, Japan. The authors thank Dr. Y. Sakuma for helpful discussion of the growth mechanism of GeMCs.

Supporting Information Available: EDX spectra and STEM image taken from the particle (area 1) and nonparticle (area 2) areas in a GeMC (GeH_4:B_2H_6 = 10:2.2). This material is available free of charge *via* the Internet at http://pubs.acs.org.

REFERENCES AND NOTES

1. Li, Y.; Qian, F.; Lieber, C. M. Nanowire Electronic and Optoelectronic Devices. *Mater. Today* **2006**, *9*, 18–27.
2. Thelander, C.; Agarwal, P.; Brongersma, S.; Eymery, J.; Feiner, L. F.; Forchel, A.; Scheffler, M.; Riess, W.; Ohlsson, B. J.; Gösele, U.; Samuelson, L. Nanowire-Based One-Dimensional Electronics. *Mater. Today* **2006**, *9*, 28–35.
3. Pauzauskie, P. J.; Yang, P. Nanowire Photonics. *Mater. Today* **2006**, *9*, 36–45.
4. Fan, H. J.; Werner, P.; Zacharias, M. Semiconductor Nanowires: From Self-Organization to Patterned Growth. *Small* **2006**, *2*, 700–717.
5. Wang, Z. L.; Song, J. Piezoelectric Nanogenerators Based on Zinc Oxide Nanowire Arrays. *Science* **2006**, *312*, 242–246.
6. Adhikari, H.; Marshall, A. F.; Chidsey, C. D. E.; McIntyre, P. C. Germanium Nanowires Epitaxy: Shape and Orientation Control. *Nano Lett.* **2006**, *6*, 318–323.
7. Tutuc, E.; Guha, S.; Chu, J. O. Morphology of Germanium Nanowires Grwon in Presence of B_2H_6. *Appl. Phys. Lett.* **2006**, *88*, 043113.
8. Jin, C. B.; Yang, J. E.; Jo, M. H. Shape-Controlled Growth of Single Crystalline Ge Nanostructures. *Appl. Phys. Lett.* **2006**, *88*, 193105.
9. Jagannathan, H.; Deal, M.; Nishi, Y.; Woodruff, J.; Chidsey, C.; McIntyre, P. C. Nature of Germanium Nanowire Heteroepitaxy on Silicon Substrates. *J. Appl. Phys.* **2006**, *100*, 024318.
10. Sutter, E.; Sutter, P. Phase Diagram of Nanoscale Alloy Particles Used for Vapor−Liquid−Solid Growth of Semiconductor Nanowires. *Nano Lett.* **2008**, *8*, 411–414.
11. Greytak, A. B.; Lauhon, L. J.; Gudliksen, M. S.; Lieber, C. M. Growth and Transport Properties of Complementary Germanium Nanowire Field-Effect Transistors. *Appl. Phys. Lett.* **2004**, *84*, 4176–4178.
12. Hanrath, T; Korgel, B. A. A Comprehensive Study of Electron Energy Losses in Ge Nanowires. *Nano Lett.* **2004**, *4*, 1455–1461.
13. Tutuc, E.; Appenzeller, J; Reuter, M. C.; Guha, S. Realization of a Linear Germanium Nanowire p−n Junction. *Nano Lett.* **2006**, *6*, 2070–2074.
14. Tutuc, E.; chu, J. O.; Ott, J. A.; Guha, S. Doping of Germanium Nanowires Grown in Presence of PH_3. *Appl. Phys. Lett.* **2006**, *89*, 263101.
15. Woodruff, J. H.; Ratchford, J. B.; Goldthorpe, I. A.; McIntyre, P. C.; Chidsey, C. E. D. Vertically Oriented Germanium Nanowires Grown from Gold Colloids on Silicon Substrates and Subsequent Gold Removal. *Nano Lett.* **2007**, *7*, 1637–1642.
16. Lauhon, L. J.; Gudiksen, M. S.; Wang, D.; Lieber, C. M. Core-Multishell Nanowire Heterostructures. *Nature* **2002**, *420*, 57–61.
17. Xiang, J.; Lu, W.; Hu, Y.; Wu, Y.; Yan, H.; Lieber, C. M. Ge/Si Nanowire Heterostructures As High-Performance Field-Effect Transistors. *Nature* **2006**, *441*, 489–493.
18. Fukata, N.; Chen, J.; Sekiguchi, T.; Okada, N.; Murakami, K.; Tsurui, T.; Ito, S. Doping and Hydrogen Passivation of B in Silicon Nanowires Synthesized by Laser Ablation. *Appl. Phys. Lett.* **2006**, *89*, 203109.
19. Fukata, N.; Chen, J.; Sekiguchi, T.; Matsushita, S.; Oshima,

T.; Uchida, N.; Murakami, K.; Tsurui, T.; Ito, S. Phosphorus Doping and Hydrogen Passivation of Donors and Defects in Silicon Nanowires Synthesized by Laser Ablation. *Appl. Phys. Lett.* **2007**, *90*, 153117.
20. Fukata, NImpurity Doping in Silicon Nanowires. *Adv. Mater.* **2009**, *21*, 2829–2832.
21. Fukata, N.; Mitome, M.; Bando, Y.; Seoka, M.; Matsushita, S.; Murakami, K.; Chen, J.; Sekiguchi, T. Codoping of Boron and Phosphorus in Silicon Nanowires Synthesized by Laser Ablation. *Appl. Phys. Lett.* **2008**, *93*, 203106.
22. Cui, Y.; Lauhon, L. J.; Gudiksen, M. S.; Wang, J.; Lieber, C. M. Diameter-Controlled Synthesis of Single-Crystal Silicon Nanowires. *Appl. Phys. Lett.* **2001**, *78*, 2214–2216.
23. Wu, Y.; Cui, Y.; Huynh, L.; Barrelet, C. J.; Bell, D. C.; Lieber, C. M. Controlled Growth and Structures of Molecular-Scale Silicon Nanowires. *Nano Lett.* **2004**, *4*, 433–436.
24. Ma, D. D. D.; Lee, C. S.; Au, F. C. K.; Tong, S. Y.; Lee, S. T. Small-Diameter Silicon Nanowire Surfaces. *Science* **2003**, *299*, 1874–1877.
25. Hannon, J. B.; Kodambaka, S.; Ross, F. M.; Tromp, R. M. The Influence of the Surface Migration of Gold on the Growth of Silicon Nanowires. *Nature* **2006**, *440*, 69–71.
26. Hetrog, M. I.; Rouviere, J. L.; Dhalluin, F.; Desre, P. J.; Gentile, P.; Ferret, P.; Oehler, F.; Baron, T. Control of Gold Surface Diffusion on Si Nanowires. *NanoLett.* **2008**, *8*, 1544–1550.
27. Barth, S.; Estrade, S.; Hernandez-Ramirez, F.; Peiro, F.; Arbiol, J.; Romano-Rodriguez, A.; Morante, J. R.; Mathur, S. Studies on Surface Facets and Chemical Composition of Vapor Grown One-Dimensional Magnetite Nanostructures. *Cryst. Growth Des.* **2009**, *9*, 1077–1081.
28. Richter, H.; Wang, Z. P.; Ley, L. The One-Phonon Raman Spectrum in Microcrystalline Silicon. *Solid State Commun.* **1981**, *39*, 625–629.
29. Campbell, I. H.; Fauchet, P. M. The Effects of Microcrystal Size and Shape on the One Phonon Raman Spectra of Crystalline Semiconductors. *Solid State Commun.* **1986**, *58*, 739–741.
30. Fukata, N.; Oshima, T.; Murakami, K.; Kizuka, T.; Tsurui, T.; Ito, S. Phonon Confinement Effect of Silicon Nanowires Synthesized by Laser Ablation. *Appl. Phys. Lett.* **2005**, *86*, 213112.
31. Fano, U. Effects of Configuration Interaction on Intensities and Phase Shifts. *Phys. Rev.* **1961**, *124*, 1866–1878.
32. Olego, D.; Cardona, M. Self-Energy Effects of the Optical Phonons of Heavily Doped p-GaAs and p-Ge. *Phys. Rev. B* **1981**, *23*, 6592–6602.
33. Morral, A. F. I.; Arbiol, J.; Prades, J. D.; Cirera, A.; Morante, J. R. Synthesis of Silicon Nanowires with Wurtzite Crystalline Structure by Using Standard Chemical Vapor Deposition. *Adv. Mater.* **2007**, *19*, 1347–1351.
34. Gupta, R.; Xiong, Q.; Adu, C. K.; Kim, U. J.; Eklund, P. C. Laser-Induced Fano Resonance Scattering in Silicon Nanowires. *Nano Lett.* **2003**, *3*, 627–631.
35. Chandrasekhar, M.; Renucci, J. B.; Cardna, M. Effects of Interband Excitations on Raman Phonons in Heavily Doped n-Si. *Phys. Rev. B* **1978**, *17*, 1623–1633.
36. Erwin, S. C.; Zu, L.; Haftel, M. I.; Efros, A. L.; Kennedy, T. A.; Norris, D. J. Doping Semiconductor Nanocrystals. *Nature* **2005**, *436*, 91–94.
37. Dalpian, G. M.; Chelikowsky, J. R. Self-Purification in Semiconductor Nanocrystals. *Phys. Rev. Lett.* **2006**, *96*, 226802.
38. Perea, D. E.; Hemesath, E. R.; Schwalbach, E. J.; Lensch-Falk, J. L.; Voorhees, P. W.; Lauhon, L. J. Direct Measurement of Dopant Distribution in an Individual Vapour−Liquid−Solid Nanowires. *Nat. Nanotechnol.* **2009**, *4*, 315–319.
39. Piscanec, S; Cantoro, M; Ferrari, A. C.; Zapien, J. A.; Lifshitz, Y.; Lee, S. T.; Hofmann, S.; Robertson, J. Raman Spectroscopy of Silicon Nanowires. *Phys. Rev. B* **2003**, *68*, 241312(R).
40. Fukata, N.; Oshima, T.; Okada, N.; Kizuka, T.; Tsurui, T.; Ito, S.; Murakami, K. Phonon Confinement and Self-Limiting Oxidation Effect of Silicon Nanowires Synthesized by Laser Ablation. *J. Appl. Phys.* **2006**, *100*, 024311.